Robotica (2002) volume 20, pp. 291–298. © 2002 Cambridge University Press
DOI: 10.1017/S0263574701003691 Printed in the United Kingdom

Path planning for non-holonomic vehicles: a potential viscous fluid field method

C. Louste* and A. Liégeois†

LIRMM – UMR 5506 CNRS/Université Montpellier II, 161 rue Ada – 34392 Montpellier CEDEX 5 (France)
** E-mail: clouste@yahoo.fr; † E-mail: liegeois@lirmm.fr*

(Received in Final Form: July 23, 2001)

SUMMARY

This paper deals with the path planning of non-holonomic vehicles on an uneven natural terrain. It uses the properties of incompressible viscous fluid fields. The full configuration is considered including position and orientation. Lanes are computed instead of a single path. Bounds on curvature and constraints on initial and final orientations are also addressed. By using the Keymeulen/Decuyper fluid method and adding friction forces in the Stokes' equations, the shortest paths or the minimum energy ones can be found, even on an uneven terrain. In addition, in order to satisfy the kinematics and dynamics constraints of a non-holonomic robot a local variation of the shear constraint is used to control the upper bound of the trajectory curvature. Adding small corridors at the departure and destination also satisfies initial and final orientation requirements.

KEYWORDS: Mobile robots; Non-holonomic path planning; Potential methods; Incompressible viscous fluids.

1. INTRODUCTION

Driving a mobile robot toward a target through an obstacle field remains a fundamental problem in robotics. Path planning methods are usually classified into two categories: graph methods and potential field methods.[1,2] Graph methods are based on a geometrical cell-decomposition of space. These methods require large computation resources that produces optimum path planning with respect to objective criteria, such as finding the shortest, or the minimum energy path.[3,4]

The potential field methods, pioneered by Kathib,[5] consist in applying physical models to the robot and its environment. Khatib's method was developed from an analogy with electrostatic field physics where obstacles generate a repulsive field, while the desired destination emits an attractive field. A key problem with this approach is that the robot gets often trapped in a local minimum.

Two research areas issued from that study. A first way has developed methods to allow the robot to escape local minima[6] or, better, to avoid them.[7] Kodischek and Rimon opened the second important area in proposing potential navigation functions that eliminate local minima (except arrival) for spherical obstacles.[8,9] However, extension to more general obstacle shapes has proved to be difficult.

In the same way, Connoly, Burns and Weiss[10] proposed a potential field based on Laplace's equation. They demonstrated that this potential field has no local minima. The study of Laplace's equation was completed by Masoud et al.[11] and Kim ahd Khosla.[12]

Other physical analogies have been proposed, more particularly a magnetic analogy developed by Singh,[13] a scent diffusion model presented by Schmidt,[14] and a method using principles in fluid dynamics proposed by Keymeulen.[15]

These potential methods do not produce an optimum energy consumption path. Furthermore most of paths planning methods have ignored the non-holonomic behaviour of robots. When taken into account, nonholonomic constraints are post processed.

To avoid the drawbacks of the existing methods, this paper deals with a road planning strategy based on Stokes' equations for incompressible viscous fluids. Section 2 recalls the advantages of general fluid methods, such as ensuring robot security and non-existence of local minima. Keymeulen and Decuyper[16,17] showed these properties.

Section 3 proposes optimum path planning with various performance indices. Indeed, introducing external friction forces into the initial model allows the selection of optimised roads. Two friction forces are defined: The first one is used to select the shortest paths; the second shows the minimum energy lanes. An example on an uneven natural terrain is given, which illustrates the performance. Section 4 presents the way to deal with kinematic and dynamic constraints by controlling the local deformation of fluid particles to obtain a lower bound to the stream lines radius of curvature.

2. FLUID METHODS

Fluid methods, pioneered by Keymeulen and Decuyper, have many properties.[16] First, these authors demonstrate that fluid methods generate a collision free path from a fluid vector field which is not necessarily the gradient of a potential function. Second, they prove that using fluid flow for path generation does not produce any local minima but unstable stagnation points on obstacles, and how a local pressure field guides fluid particles and finds the shortest path. Third, they analyse the interplay between the dynamical laws and boundary conditions using tools from topology. The Dirichlet and Von Newmann boundary conditions are studied.

In conclusion, they show that the best planning result can be obtained by using incompressible viscous fluids. The viscosity implies that the velocity is zero on the boundary[18]

and maximum at the center of the fluid tubes bordered by obstacles.[17]

The selection of the path consists in a streamline computed as the line where the shear stress tensor field in the direction of velocity is zero. This streamline has the maximum velocity.

2.1. Stokes' equations

According to Keymeulen and Decuyper's results we propose a method based on an incompressible and very viscous fluid described by the Stokes' equations for stationary flow and we develop improvements to include kinematical and geometrical constraints.

The Stokes' equations are:

$$\mu\Delta\vec{v}=\vec{\nabla}p-\vec{f} \tag{1}$$

$$\vec{\nabla}\bullet\vec{v}=0 \tag{2}$$

where:

$\vec{v}$ is the velocity vector
$\vec{f}$ is the vector of the external forces acting on the particle
p is the local pressure
μ is the viscosity coefficient
Δ represents the Laplace's operator
$\vec{\nabla}$ is the spatial derivation vector (the gradient operator)
• symbolises the scalar product.

2.2. High-viscosity advantages

First vortices can exist only in a low-viscosity domain. As it is shown in Figure 1, vortices c_1, c_2, c_3, c_4 result from inertial forces.

The initial Stokes' hypotheses are that mechanical forces are negligible and that viscous forces are large. Therefore no vortex can exist (Figure 2).

Moreover, in a high-viscosity fluid, the speed of a particle decreases when approaching an obstacle and becomes zero on the boundary between fluid and obstacle. This property ensures safety for robots. Indeed, because of viscous forces, by following the streamline defined with a shear stress tensor field equal to zero in the direction of velocity, a robot navigates in the middie of the fluid tubes (roads) bordered by obstacles.[17]

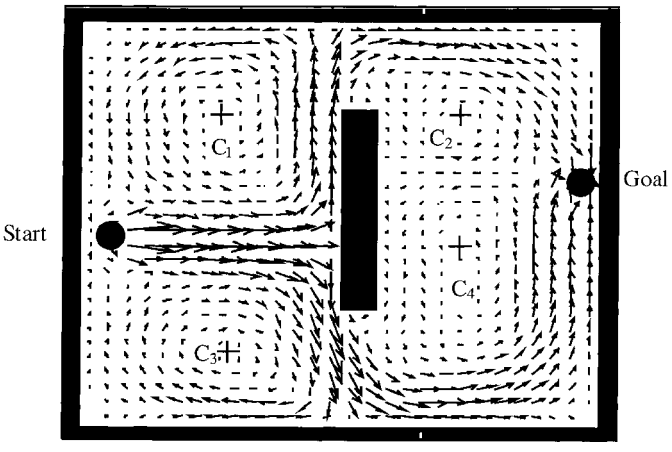

Fig. 1. Fluid velocity model with non-negligible inertial forces.

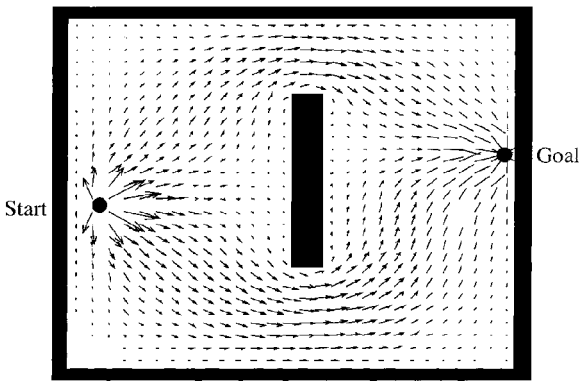

Fig. 2. Stokes' fluid velocities.

2.3. Stationary flow

In the model defined by equations (1) and (2), there are no time-dependent terms, so the equations are simple.

General properties:

- A regular grid covering obstacles and free space models the environment.

A finite difference method is used for solving the Stokes' equations.

$$\frac{v_{1i+1,j}+v_{1i,j+1}-4v_{1i,j}+v_{1i,j-1}+v_{1i-1,j}}{h^2}+f_{1i,j}=\frac{p_{i+1,j}-p_{i-1,j}}{2h} \tag{3}$$

$$\frac{v_{2i+1,j}++v_{2i,j+1}-4v_{2i,j}+v_{2i,j-1}+v_{2i-1,j}}{h^2}+f_{2i,j}=\frac{p_{i+1,j}-p_{i-1,j}}{2h} \tag{3}$$

$$v_{1i+1,j}-v_{1i-1,j}+v_{2i,j+1}-v_{2i,j-1}=0 \tag{5}$$

where (v_1, v_2) are the velocity co-ordinates, (f_1, f_2) the external force co-ordinates and p the pressure. The boundary conditions are zero velocities on the obstacle boundaries and on the limits of the closed-fluid universe. A constant difference of pressure is kept between the start point and the arrival point.

- If N is the number of grid nodes, resolving our problem consists in solving a set of 3*N sparse linear equations (equations 3–5).

The simulation shown in Figure 3 confirms that the flow from the starting point to the arrival does not enter blind alleys and that no vortex is present.

3. OPTIMUM PATH PLANNING

In this section, we show how our potential method can be used to find the shortest path, or the minimum energy one, by using friction forces in the model.

In the previous section, external forces were considered to be zero. Let us now study any fluid particle during its travel from the starting point to the arrival; S is the starting point and G is the goal point (Figure 4).

By following a particle along its streamline (equation 6), we notice that its total potential energy is equal to the

https://doi.org/10.1017/S0263574701003691 Published online by Cambridge University Press

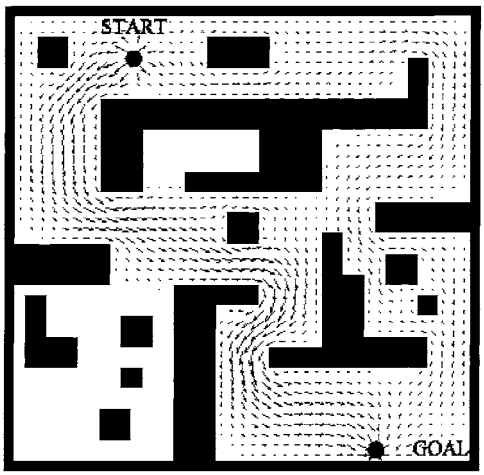

Fig. 3. A point to point viscous fluid method example.

difference of pressure between the starting and the arrival points. One has

$$\int_S^G \mu\Delta\vec{v} \bullet \vec{T} = \int_S^G \vec{\nabla}p \bullet \vec{T} \tag{6}$$

$$\int_S^G \mu\Delta\vec{v} \bullet \vec{T}\, ds = p_G - p_S \tag{7}$$

where $\vec{T}$ is the trajectory tangent vector and $p_G - p_S$ is the pressure difference between G and S. Two terms are in evidence in the equation 7: The first one is the global pressure difference and the second one is the viscosity forces work.

As walls and obstacles are motionless, viscosity forces slow down fluid particles and so the viscosity forces work between G and S is negative (equation 8).

$$W_u = \int_S^G \mu\vec{v} \bullet \vec{T}\, ds \leq 0 \tag{8}$$

In conclusion, the more a particle is far from obstacles, the faster it travels, i.e. in the middle of canal.

3.1. The shortest path

Let us add an external friction force $\vec{F}$ in the model. This force has the direction opposite to the velocity vector and its value is assumed here to remain constant all over the domain (Figure 5).

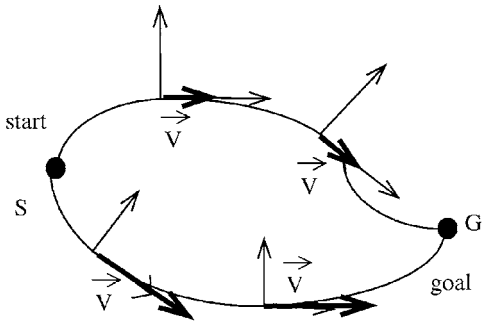

Fig. 4. Streamlines examples without friction.

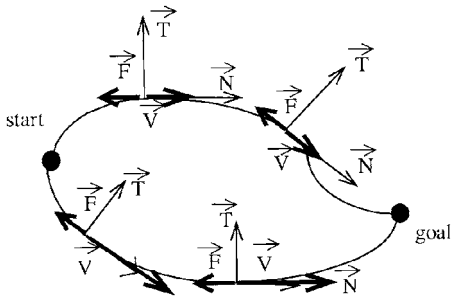

Fig. 5. Streamlines with friction force.

Now, energy is not only dissipated by viscous forces but by friction forces too. By following a particle along its streamline, we notice that the mechanical work of friction forces ($L \bullet F$) depends on the length L of the particle trajectory (equations 9 and 10).

$$\int_S^G \mu\Delta\vec{v} \bullet \vec{T} + \int_S^G \vec{F} \bullet \vec{T} = \int_S^G \vec{\nabla}p \bullet \vec{T} = p_G - p_S \tag{9}$$

$$W_u - L \bullet F = p_G - p_S \tag{10}$$

As the viscous forces work W_u is negative and as the potential energy due to the difference of pressure $p_G - p_S$ is constant (equation 11), adding a constant friction force F modifies the flow line shapes. All streamlines in the solution have a bounded length (equation 12).

$$W_u \leq 0 \quad p_G - p_S + LF \leq 0 \tag{11}$$

$$L \leq L_{limit} = \frac{p_S - p_G}{F} \tag{12}$$

When a fluid flow problem has no solution, the fluid particle velocity is zero all over the domain. So, by iteration, it is possible to quickly find F_{max} and L_{min} (equation 13), respectively, the maximal value of F and the minimal value of L, accepting at least a non-zero particle velocity. This particle follows the shortest trajectory.

$$L_{min} = \frac{p_S - p_G}{F_{max}} \tag{13}$$

In practice, the width of the solution paths can't be shorter than four grid nodes due to the approximation of the finite difference method (Figure 6). Moreover, we never consider the shortest trajectory because it gets very close to obstacle corners, which is dangerous for a robot. We prefer to compute lanes wider than the robot width (Figure 7). In order to illustrate advantages of the fluid method, we have proposed a comparison between our method and another typical potential fluid method (the scent diffusion[21]) proposed by G. Schmidt.

Our method also allows us to find the shortest paths on an uneven terrain by using its elevation map (Figure 8). In this case, the problem comes from the distance projection onto the map. We keep the friction forces with an opposite direction to the direction of motion with a constant norm F along the real trajectory.

https://doi.org/10.1017/S0263574701003691 Published online by Cambridge University Press

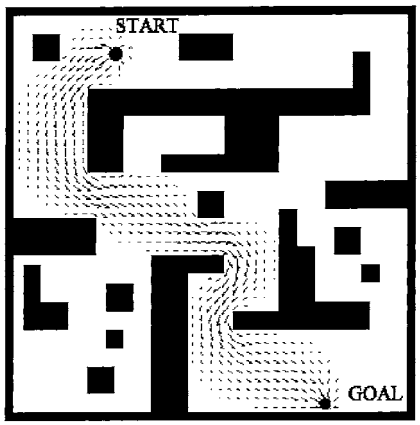

Fig. 6. Shortest stream canal in a point to point example.

Let L_r be the length of the real trajectory and L_p the length of the projected trajectory. The mechanical work exerted by the friction force must be the same on the real trajectory and on the trajectory projection. So we use a non-constant friction force F_c in the map to correct the projection effects.

$$W_r = W_p \Leftrightarrow F.L_r = F_c.L \tag{14}$$

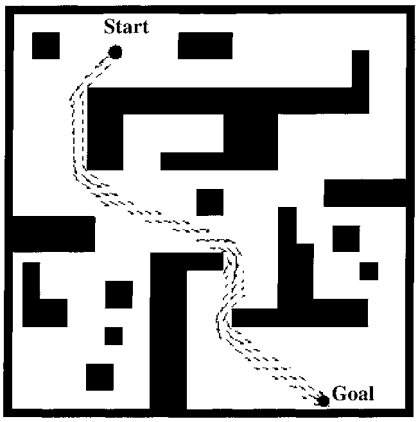

Fig. 7. Near-optimal canal.

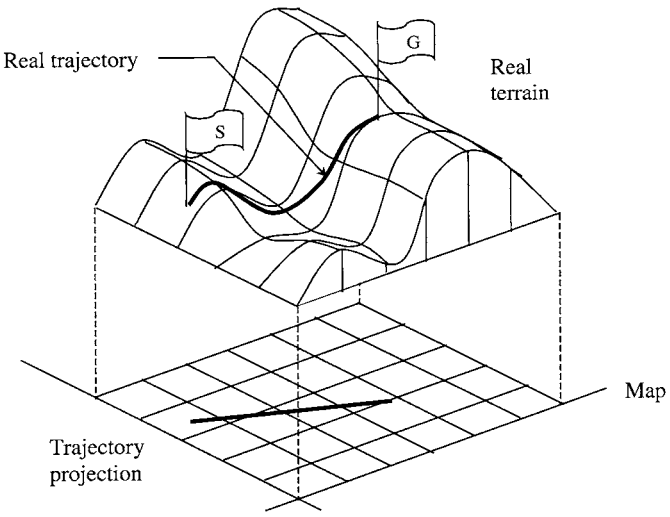

Fig. 8. A real trajectory and its projection.

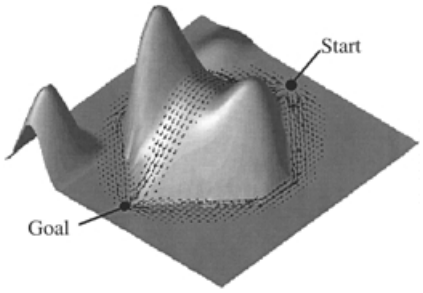

Fig. 9. The three equivalent shortest roads.

where W_r is the mechanical work exerted along the real trajectory and W_p the mechanical work exerted on the projected trajectory.

$$dW_r = dW_p \Leftrightarrow F.dL_r = F_c.dL_p \tag{15}$$

α is the angle of the slope.

$$dL_p = \cos\alpha.dL_r \tag{16}$$

$$F_c = \frac{F}{\cos\alpha} \tag{17}$$

The example (Figures 9 and 10) shows the path planning on an uneven terrain.

We notice that the three paths with the same length are found.

3.2. The minimum energy consumption path

Energy consumption is a typical problem for robotic autonomous rovers. Hence a robot navigating on uneven surfaces has to minimise its energy consumption.

Like in the preceding section, an external force is used to simulate the robot's energy consumption. A complete model should take into account the relationship between engine power, speed, gear efficiency, wheels contact and so on.

Here we present a simple model based on energy variation when a mass is moving on uneven surfaces.

$$f = mg(|\tan\gamma| + K_f) \tag{18}$$

m is the vehicle mass

g is the gravity

γ is the angle representing the slope in the direction of motion

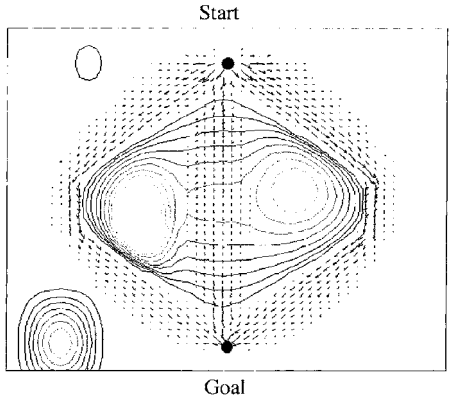

Fig. 10. The three shortest roads and the contour lines.

https://doi.org/10.1017/S0263574701003691 Published online by Cambridge University Press

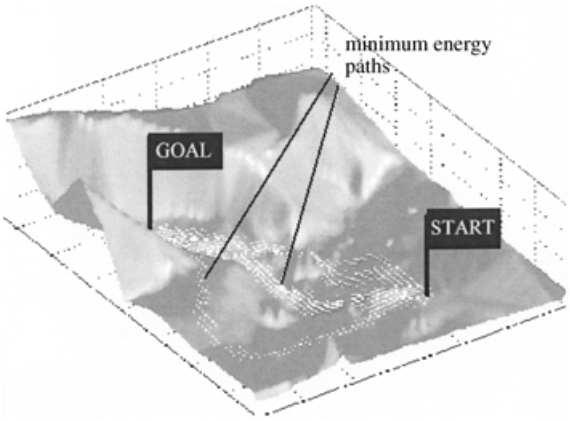

Fig. 11. A 3D representation of the minimum energy consumption paths on the GEROMS site.

K_f is friction coefficient between the wheels and the ground

The example (Figure 11) presents the GEROMS experimental site[19] (about 60*100m). The ground represents a part of the moon surface including pits, smooth hills and rocks. Rocks and steep terrain are considered as obstacles. Three paths are found: Two of them go through the pit and the third turns around it and follows a contour line. Pinchard[4] has proposed a comparison with path generation based on the principles of genetic algorithms.

4. PATH PLANNING FOR NON-HOLONOMIC ROBOT

A real robot is not able to follow any trajectory. Inertial forces and mechanical limits force the robot to follow trajectories with a bounded curvature:

$$\kappa = \frac{1}{R} \tag{19}$$

where R is the local radius of curvature (Figure 12).

$\vec{T}$ and $\vec{N}$ are, respectively, the tangent and the normal vector to a trajectory.

The relation between the curvature K, the velocity and the heading θ is:

$$\kappa = \frac{\left| \left(\frac{\partial v_2}{\partial x_2} - \frac{\partial v_1}{\partial x_1} \right) \sin\theta \cos\theta - \frac{\partial v_1}{\partial x_2} \sin^2\theta + \frac{\partial v_2}{\partial x_1} \cos^2\theta \right|}{\| \vec{v} \|} \tag{20}$$

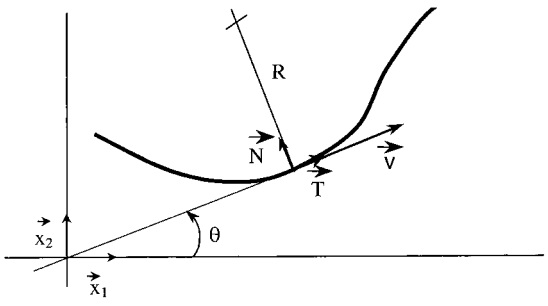

Fig. 12. Radius of curvature.

In this section we introduce a constraint in our model in order to control the curvature of the trajectories. In this way, we guarantee that a mobile robot can follow any particle.

A fluid particle which moves in a complex environment, is affected by a combination of deformations like elongation, crushing shear but no extension or compression because our assumption of fluid incompressibility (Figure 13).

According to the Stokes' equations (equations 21) when a fluid particle is turning, its shape is modified (Figure 14).

$$\begin{aligned} \vec{\vec{\sigma}} &= -p\vec{\vec{I}} + 2\mu\vec{\vec{D}} \\ d\vec{i}v &= \vec{\vec{\sigma}} + \vec{f} = \vec{0} \\ div &= \vec{v} = 0 \end{aligned} \tag{21}$$

where $\vec{\vec{I}}$ is the identity tensor, $\vec{\vec{D}}$ the deformation rate tensor, and μ the viscosity coefficient.

We call the perpendicular shear rate $\sigma_{\eta\varepsilon}$ the deformation movement in the direction perpendicular to the particle motion (Figure 14).

$$\sigma_{\eta\varepsilon} = \frac{\partial v_\eta}{\partial \varepsilon} \tag{22}$$

$$\vec{v} = v_\varepsilon \vec{\varepsilon} + v_\eta \vec{\eta} \tag{23}$$

where $(0, \vec{\varepsilon}, \vec{\eta})$ is a local normalised reference frame where

$$\vec{\varepsilon} = \frac{\vec{v}}{\| \vec{v} \|} \tag{24}$$

There is a direct relationship between local normal shear deformation movement and the curvature of a trajectory.

$$\left| \frac{\partial v_\eta}{\partial \varepsilon} \right| = \kappa \| \vec{v} \|$$

$$= \left| \left(\frac{\partial v_2}{\partial x_2} - \frac{\partial v_1}{\partial x_1} \right) \sin\theta \cos\theta - \frac{\partial v_1}{\partial x_2} \sin^2\theta + \frac{\partial v_2}{\partial x_1} \cos^2\theta \right| \tag{25}$$

Now we can introduce a new tensor $\vec{\vec{G}}$. $G_{x1,x2}$ represents the corresponding matrix in the absolute reference frame.

$$G_{x_1,x_2} = \begin{bmatrix} -\frac{\partial v_\eta}{\partial \varepsilon} \cos\theta \sin\theta & -\frac{\partial v_\eta}{\partial \varepsilon} \sin^2\theta \\ \frac{\partial v_\eta}{\partial \varepsilon} \cos^2\theta & \frac{\partial v_\eta}{\partial \varepsilon} \cos\theta \sin\theta \end{bmatrix} \tag{26}$$

The stress produced by the constraint tensor $\vec{\vec{G}}$ on a particle frontier is by definition equal to

$$\vec{F} = \vec{\vec{G}} \bullet \vec{n} \tag{27}$$

where $\vec{n}$ is the normal vector at the surface of a fluid particle

$$\vec{n} = a\vec{\varepsilon} + b\vec{\eta}$$

$$\vec{F} = \vec{\vec{G}} \bullet \vec{n} = \begin{bmatrix} -a \sin\theta \frac{\partial v_\eta}{\partial \varepsilon} \\ a \cos\theta \frac{\partial v_\eta}{\partial \varepsilon} \end{bmatrix}_{x_i,x_2} = \begin{bmatrix} 0 \\ a \frac{\partial v_\eta}{\partial \varepsilon} \end{bmatrix}_{\varepsilon\eta} \tag{28}$$

https://doi.org/10.1017/S0263574701003691 Published online by Cambridge University Press

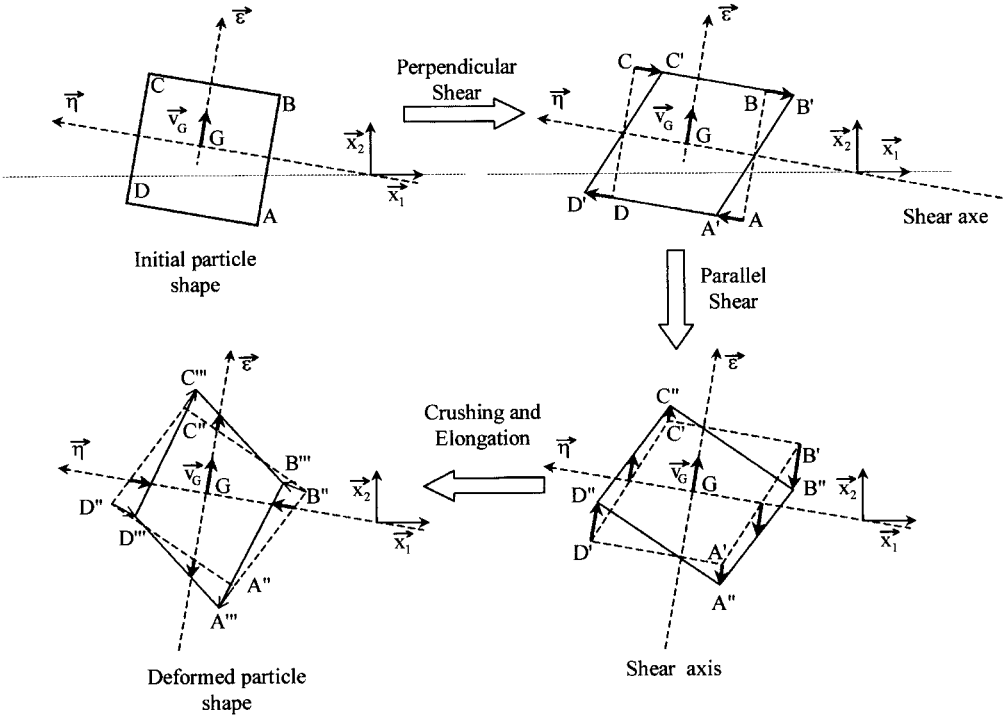

Fig. 13. Combination of deformations expressed in the local frame $(0, \vec{\varepsilon}, \vec{\eta})$.

$$\forall \vec{v} \text{ and } \forall \vec{n}, \vec{F} \bullet \vec{v} = 0$$

The $\vec{\vec{G}}$ tensor produces a force $\vec{F}$ opposite to the deformation (Figure 15).

We define a new tensor $\vec{\vec{\sigma}}'$ by adding a term to the Stokes' equation:

$$\vec{\vec{\sigma}}' = -p\vec{\vec{I}} + 2\mu\vec{\vec{D}} + k(\vec{x})\vec{\vec{G}} \tag{29}$$

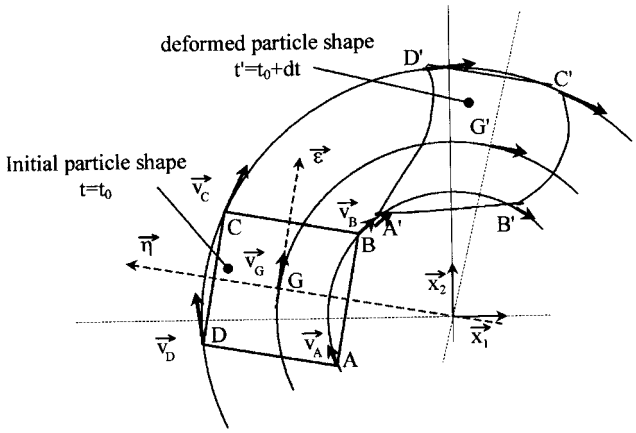

Fig. 14. Shape of a particle in a turn.

where $\vec{\vec{I}}$ is the identity tensor, $\vec{\vec{D}}$ the deformation rate tensor, μ the viscosity coefficient, and k the curve coefficient depending on the local position.

By using local internal constraints opposite to shear, we can control local fluid particle deformations and consequently the global fluid direction (Figure 16). To influence the particle direction, a different value of the stress coefficient k is used.

New global equations are then defined:

$$\overrightarrow{\text{div}}\,\vec{\vec{\sigma}}' + \vec{F} = \vec{0} \tag{30}$$

$$\text{div}\,\vec{v} = 0 \tag{31}$$

With the following additional constraint:

$$\left| \frac{\dfrac{\partial v_\eta}{\partial \varepsilon}}{\|\vec{v}\|} \right| < \kappa_{\max}$$

where K_{max} is the upper bound of the curvature.

By this method, roads with a bounded curvature radius are obtained (Figure 18), to be compared with the classical simplest Stokes' equation (Figure 17).

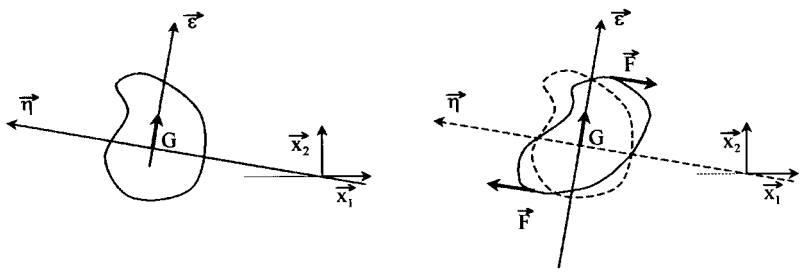

Fig. 15. Controlling the shape of a particle by a force.

https://doi.org/10.1017/S0263574701003691 Published online by Cambridge University Press

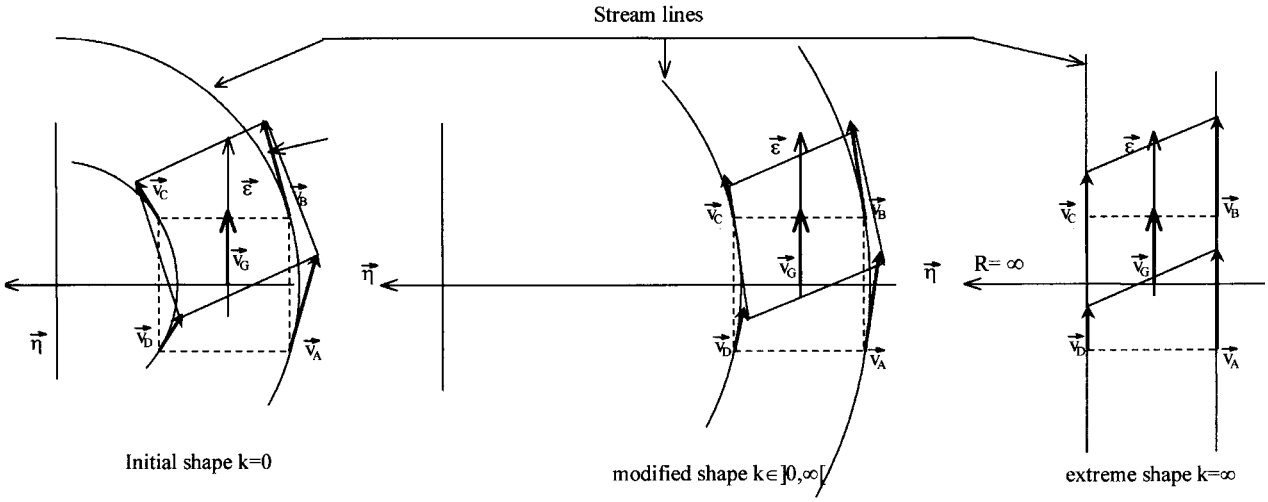

Fig. 16. Example of particle shapes with different values of k.

5. INITIAL AND FINAL ORIENTATION CONSTRAINTS

A non-holonomic robot is only able to start in a limited range of directions (Figure 19). In order to model this constraint, we limit the fluid direction around the starting and arrival points. Our solution is to build a virtual wall all around these points (Figure 20).

Figure 21 shows a safe path planning with a lower bound of the radius of curvature.

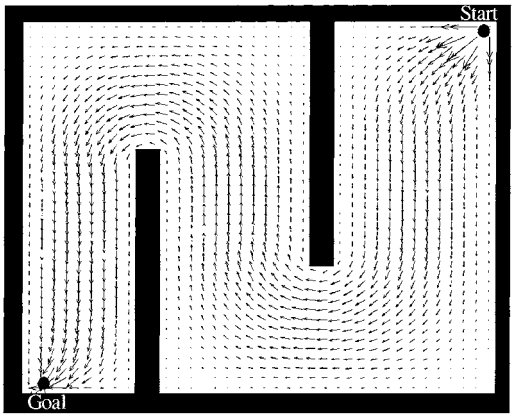

Fig. 17. Road planning with the classical Stokes' equations.

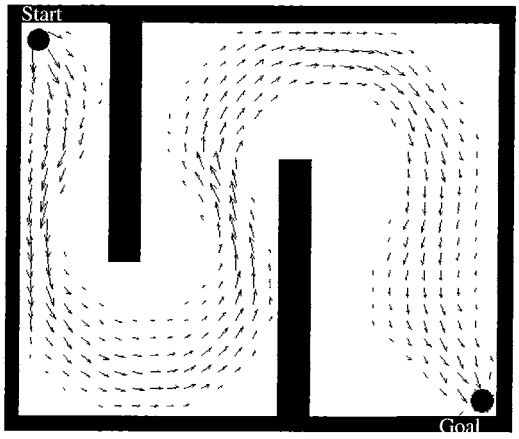

Fig. 18. Road planning with a bounded curvature.

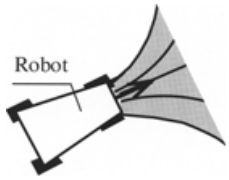

Fig. 19. Mechanical limits of a non-holonomic vehicle.

Imposing a bounded radius, the problem may have no solution. In such cases, the velocity vectors are null all over the domain. So we can easily predict the existence or non-existence of a feasible solution.

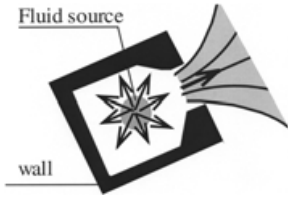

Fig. 20. Oriented fluid source.

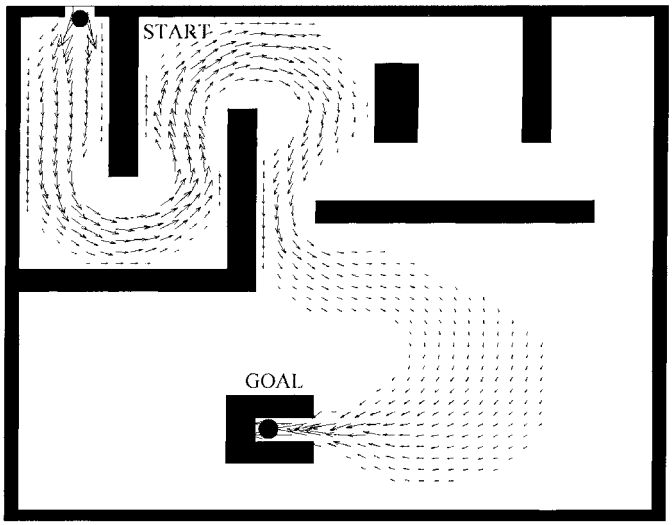

Fig. 21. Road with a bounded radius and a constrained final orientation.

https://doi.org/10.1017/S0263574701003691 Published online by Cambridge University Press

6. CONCLUSION

In this paper we have presented an original incompressible viscous fluid method for generating safe paths between two points in a complex environment.

Paths correspond to the speediest flow of fluid particles. We have discussed the advantages of a viscous fluid approach. An unwanted local attractor is not generated but unstable stagnation points and the security of the robot are guaranteed.

We have argued that using external forces allows the planning of safe paths, which can be optimal with respect to distance or energy criteria.

Furthermore, since a real mobile robot cannot follow arbitrary trajectories, because of mechanical limits or inertial forces, we have proposed a method based on an internal force, in order to control the minimum radius of the computed stream lines.

The method is a way to obtain preferential lanes for indoors as well as for outdoors non-holonomic mobile robots.

ACKNOWLEDGEMENTS

The authors would like to thank the referees for their very constructive and detailed comments and suggestions.

References

1. J. Barraquand, B. Langlois and J-C. Latombe, "Numerical Potential Field Techniques for Robot Path Planning", *IEEE Trans. on S.M.C.* **22**, No. 2, 224–241 (1992).
2. Y.K. Hwang and N. Ahuja, "Cross motion planning – a Survey", *ACM Computer Survey* **24**, No. 3, 1–6 (1992).
3. O. Pinchard and A. Liǵeois, "Non Deterministic Methods for Robot Path Planning in the Presence of Uncertainties' ", *Proc. of CESA '96 IMACS Multiconference (Robotics and Cybernetics)*, Lille, France (1996) pp. 593–598.
4. O. Pinchard, A. Liégeois and T. Emmanuel, "A Genetic Algorithm for Outdoor Robot Path Planning", *Proc. of the 4th Int. Conf on Intelligent Autonomous Systems*, IOS Press, Karlsruhe (1995) pp. 413–419.
5. O. Khatib and J.F. Le Maître, "Dynamic Control of Manipulators Operating in a Complex Environment", *Proc of the 3rd ClSM-1FToMM Symp. On the Theory and Practice of Robots and Manipulators*, Udine (1978) pp. 267–282.
6. H. Chang, "A New Technique To Handle Local Minimum For Imperfect Potential Field Based Motion Planning", *Proc. IEEE Int. Conf on Robotics and Automation*, Minneapolis (1996) pp. 108–112.
7. N. Clavel, R. Zapata and F. Sevila, "Non-holonomic Local Navigation by Means of Time and Speed Dependent Artificial Potential Fields", *Proc lEEE Int. Conf on Intelligent Robots Systems"*, Yokohama, Japan (1993), **Vol. 3**, pp. 2272–2278.
8. D.E. Koditschek, "Exact Robot Navigation by Means of Potential Functions: Some Topological Considerations", *Proc. IEEE Int. Conf on Robotics and Automation*, Raleigh (1987) pp. 1–6.
9. E. Rimon and D.E. Koditschek, "Exact Robot Navigation using Cost Functions: The Case of Distinct Spherical Boundaries in E^n", *Proc. 1988 IEEE Int. Conf on Robotics and Automation*, Philadelphia (1988) pp. 1791–1796.
10. C.I. Connoly, J.B. Burns and R. Weiss, "Path Planning Using Laplace's Equation", *Proc. of the 1990 IEEE Int. Conf. on Robotics and Automation*, Cincinnati (1990) pp. 2102–2106.
11. A.A. Masoud, S.A. Masoud and M.M. Bayoumi, "Robot navigation using a pressure generated mechanical stress field: the biharmonic potential field approach", *Proc. 1994 IEEE Int. Conf. on Robotics and Automation*, San Diego (1994) 124-129.
12. J. Kim and P. Khosla, "Real-Time Obstacle Avoidance Using Harmonic Potential Functions", *Proc. IEEE Int. Conf on Robotics and Automation*, Sacramento (1991), pp. 790–796.
13. L. Singh, Stephanou Harry and J. Wen, "Real-Time Robot Motion Control with Circulatory Fields", *Proc. IEEE Int. Conf. on Robotics and Automation*, Minneapolis (1996) pp. 2737–2742.
14. G. Schmidt and W. Neubauer, "High-Speed Robot Path Planning in Time-Varying Environment Employing a Diffusion Equation Strategy" In: (S.G. Tsafestas, ed.), *Robotic Systems* (1992), pp. 207-215.
15. D. Keymeulen and J. Decuyper, "A Reactive Robot Navigation System Based on a Fluid Dynamics Metaphor", **In**: "*Parallel Problem Solving from Nature*", Lecture Notes in Computer Science (Springer-Verlag (1990) No. 496, pp. 356–362.
16. D. Keymeulen and J. Decuyper, "The Fluid Dynamics Applied to Mobile Robot Motion: The Stream Field Method", *Proc. IEEE Int. Conf on Robotics and Automation*, San Diego (1994) pp. 378–385.
17. D. Keymeulen and J. Decuyper, "Self-Organizing System for the Motion Planning Of Mobile Robots", *Proc. IEEE Int. Conf. on Robotics and Automation*, Minneapolis (1996) pp. 3369–3374.
18. I. L. Ryhming, *Dynamique des fluides* (Presses polytechniques romandes, Lavoisier diffusion, 1985).
19. M. Delail, "First Campaigns on the GEROMS Mobile Robot Test Site", *Proc. of the 2nd IARP Workshop on Robotics in Space*, Montreal, Ed. Canadian Space Agency (1994) Paper 5-7.
20. C. Louste and A. Liégeois, "Robot Path Planning Using Models of Fluid Mechanics" **In**: *Progress in System and Robot Analysis and Control Design* (S. Tsafestas and G. Schmidt, eds.) Springer (1999), Ch. 41, pp. 515–524.
21. C. Louste and A. Liégeois, "Near Optimal Robust Path Planning for Mobile Robots: the Viscous Fluid Method with Friction", *Journal of Intelligent and Robotic Systems* **27**, 99–112 (2000).

https://doi.org/10.1017/S0263574701003691 Published online by Cambridge University Press